JOURNAL OF VIROLOGY, Jan. 1996, p. 305–312 Vol. 70, No. 1
0022-538X/96/$04.00+0

Mouse Adaptation Determinants of Poliovirus Type 1 Enhance Viral Uncoating

THÉRÈSE COUDERC,[1] FRANCIS DELPEYROUX,[2] HÉLÈNE LE BLAY,[1] AND BRUNO BLONDEL[1]*

Unité de Neurovirologie et Régénération du Système Nerveux,[1] and Laboratoire d'Epidémiologie Moléculaire des Entérovirus,[2] Institut Pasteur, 75724 Paris Cedex 15, France

Received 21 June 1995/Accepted 16 October 1995

Most poliovirus (PV) strains, such as PV type 1/Mahoney, cannot infect the mouse central nervous system. We previously identified two determinants of mouse adaptation of PV type 1/Mahoney at positions 22 and 31 of the viral capsid proteins VP1 and VP2, respectively (T. Couderc, J. Hogle, H. Le Blay, F. Horaud, and B. Blondel, J. Virol. 67:3808–3817, 1993). These residues are located on the interior surface of the capsid. In an attempt to understand the molecular mechanisms of adaptation of PV to mice, we investigated the effects of these two determinants on the viral multiplication cycle in a human cell line. Both determinants enhanced receptor-mediated conformational changes leading to altered particles of 135S, one of the first steps of uncoating, and viral internalization. Furthermore, the residue at position 22 of VP1 appears to facilitate RNA release. These results strongly suggest that these determinants could also facilitate conformational changes mediated by the PV murine receptor and internalization in the mouse nerve cell, thus allowing PV to overcome its host range restriction. Moreover, both mouse adaptation determinants are responsible for defects in the assembly of virions in human cells and affect the thermostability of the viral particles. Thus, these mouse adaptation determinants appear to control the balance between the viral capsid plasticity needed for the conformational changes in the early steps of infection and the structural requirements which are involved in the assembly and the stability of virions.

Poliovirus (PV), the causative agent of poliomyelitis in humans, is the prototype of the genus *Enterovirus* of the family *Picornaviridae*. It is composed of a single-stranded, positive-sense RNA surrounded by an icosahedral protein shell of 60 copies of each of four capsid proteins, VP1, VP2, VP3, and VP4. The three-dimensional structure of PV has been elucidated by X-ray crystallography (13, 17). The three larger proteins, VP1, VP2, and VP3, form the outer surface; VP4 is the smallest of the capsid proteins and is confined to the inner surface of the capsid, in contact with the viral RNA and with the amino termini of VP1, VP2, and VP3. A deep depression, called the canyon, encircles each fivefold axis of symmetry. This canyon may be the binding site for the PV cellular receptor (PVR) (4, 5, 38).

There are three known serotypes of PV (PV type 1 [PV-1], PV-2, and PV-3). When injected intracerebrally, wild strains of all three PV serotypes are neurovirulent for primates. Only a few PV strains, including PV-2/Lansing, are neurovirulent in mice. The wild strain PV-1/Mahoney is highly neurovirulent in primates but does not cause paralytic disease in mice. In vitro, PV can only infect primate cells and even mouse-adapted strains cannot infect mouse L cells or any other cultured rodent cells.

The human PVR is a protein of the immunoglobulin superfamily (22, 31). The lymphocyte homing receptor CD44 may be involved in the interactions between PV and its receptor (41). The PVR performs a dual function in PV infection: attachment of the virus to the cell surface and destabilization of the virion leading to the conformational transitions that have been associated with one of the first steps in viral uncoating (11, 14–16, 20, 24). These irreversible alterations of the viral capsid include the loss of the internal capsid protein VP4 and the extrusion of the internal N terminus of VP1 (11, 15). The altered particles have a reduced sedimentation coefficient (135S versus 160S for native virions) and modified antigenic properties (11, 24). Furthermore, they are noninfectious, protease sensitive, and considerably more hydrophobic than the native virion (15, 24, 25). Early after infection, these 135S altered particles can simultaneously be found inside infected cells (11) and eluted from the cells (12, 15, 19).

The murine PVR has not been characterized. The murine genome contains a sequence homologous to the gene encoding the human PVR, but the murine PVR homolog protein isolated from cDNA clones does not function as a receptor for PV in mouse cells (32). However, murine L cells become susceptible to all strains of PV after transfection with human PVR cDNA or the human PVR gene (22, 30, 31). Moreover, transgenic mice producing human PVR are susceptible to infection with all three serotypes (23, 39).

PV strains which are not neurovirulent in mice seem therefore to be blocked at one or more of the early steps of mouse nerve cell infection. There have been many studies to identify the molecular determinants involved in host restriction of PV-1/Mahoney in mice. These determinants can be classified into two groups: (i) determinants exposed at the surface of the protein shell, i.e., the B-C loop of VP1 (amino acids 94 to 102), and residues at positions 160 of VP1, 142 of VP2, and 60 of VP3 (6, 8, 27, 37) and (ii) determinants located inside the viral capsid; i.e., the residues at positions 22, 40, 43, and 54 of VP1, 31 of VP2, and 62 of VP4 (8, 9, 34). Each of these determinants is sufficient by itself to confer a mouse-adapted phenotype to PV-1/Mahoney. In contrast, mouse neurovirulence of the mouse-adapted PV-1 strain LS-a is determined by multiple mutations in regions encoding both viral capsid protein VP1 and proteinase $2A^{pro}$ (26).

* Corresponding author. Mailing address: Unité de Neurovirologie et Régénération du Système Nerveux, Institut Pasteur, 28 rue du Docteur Roux, 75724 Paris Cedex 15, France. Phone: (33).1.45.68.87.62. Fax: (33).1.40.61.34.21. Electronic mail address: bblondel@pasteur.fr.

It has been suggested that mouse adaptation determinants are involved in the early steps of the viral cycle such that the host range of PV is extended to mice. However, the precise role of these determinants in the viral cycle has not been identified. Despite the failure to demonstrate receptor binding of either mouse-adapted or primate-specific strains to mouse brain homogenates (18), the determinants exposed at the surface of the viral capsid could influence binding to the as yet unidentified mouse receptor (8, 27, 37). The role of the internal determinants is even less clear. Colston and Racaniello (5) have shown that mutations affecting internal amino acids near a hydrocarbon-binding pocket which lies below the canyon floor in VP1 modulate PV binding. However, the internal mouse adaptation determinants are not close to this pocket, which makes it unlikely that they are involved in PV binding.

None of the available murine cell lines are susceptible to PV infection, and therefore the role of the mouse adaptation determinants cannot be elucidated by in vitro studies with such cells. As a first step to understanding how internal determinants could confer the mouse-adapted phenotype to PV-1, we used HEp-2c cells as an in vitro model to investigate effects on the viral multiplication cycle of two internal determinants of mouse adaptation that we previously identified: $VP1I_{22}$ (residue Ile-22 of VP1) and $VP2T_{31}$ (residue Thr-31 of VP2) (9). We dissected the viral multiplication cycle of the corresponding mouse-adapted PV-1/Mahoney mutants during HEp-2c cell infection. The capsid stability of these mutants was altered, allowing them to undergo more efficiently receptor-mediated conformational changes and internalization. As a corollary, capsid assembly of these mutants was less efficient. We report the first evidence of molecular changes in the viral cycle of mouse-adapted mutants, suggesting a relationship between the molecular characteristics of these mutants and their adaptation to mice.

MATERIALS AND METHODS

Cells and viruses. HEp-2c cells were grown in monolayers in modified Eagle's medium (MEM) supplemented with 5% fetal calf serum. Wild-type Mahoney strain and the mouse-adapted mutants KK-$VP1I_{22}$ and KK-$VP2T_{31}$ were derived from PV-1/Mahoney and contained amino acid substitutions Thr-22→Ile and Ser-31→Thr in the capsid proteins VP1 and VP2, respectively (9). Viruses were amplified on HEp-2c cells, and virus titers were determined by plaque assay (9). When necessary, viruses were purified by isopycnic CsCl gradient centrifugation as previously described (3).

Preparation of radiolabeled virions. Radiolabeled virions were prepared with ^{35}S[methionine] (1,000 Ci/mmol; ICN) as described previously (2) and purified by isopycnic CsCl gradient centrifugation (3). The yield of mature virions was measured optically, assuming 9.4×10^{12} particles per unit of optical density at 260 nm (40). The two mutants KK-$VP1I_{22}$ and KK-$VP2T_{31}$ and the wild-type virus were labeled with a similar specific activity (1.4×10^{-6} cpm per particle) and at a particle/PFU ratio of 850.

Plaque assay and single-cycle growth curves. Plaque assays were performed on HEp-2c cell monolayers. Infected cells were incubated for 3 days at 37°C under a 0.9% agar overlay and stained with crystal violet.

Single-cycle growth curves were obtained with HEp-2c cell monolayers (5×10^5) in duplicate 24-well dishes. Cells were infected in duplicate by incubation with virus at a multiplicity of infection (MOI) of 50 for 30 min at room temperature. Cells were then washed twice with MEM and incubated at 37°C. At intervals thereafter, plaques were taken and frozen and thawed three times to release virus from the cells. The infectious titer of each sample was determined by measuring 50% tissue culture infectious doses ($TCID_{50}$) on HEp-2c cells (29).

Binding assay. Duplicate 24-well dishes containing HEp-2c cell monolayers (5×10^5) were precooled on ice for 10 min, washed twice with ice-cold phosphate-buffered saline (PBS), and then infected with ^{35}S-labeled virions at an MOI of 50 in 0.5 ml of PBS with 0.5% bovine serum albumin (BSA) at 4°C. At various times (15, 30, 60, 90, and 120 min), the cell monolayers were washed twice with ice-cold PBS to remove unbound virus and the cells were lysed in 0.2 ml of Tris-EDTA (pH 7.6) with 0.5% sodium dodecyl sulfate (SDS) for 10 min at 37°C. Cell-associated radioactivity was then determined by scintillation counting.

Internalization kinetics. The kinetics of internalization were investigated according to the methodology described by Dietzschold et al. (10). Monolayers of HEp-2c cells were incubated in duplicate with 50 PFU of virus per cell at 37°C. After the various times as indicated, cells were washed twice with MEM and anti-PV-1 rabbit serum was added to neutralize nonattached and noninternalized virus. At 4.5 h postinfection (hpi), viral antigen in infected cells was detected by the immunofluorescent-antibody staining technique as described previously (7). Briefly, cells were washed with PBS, fixed for 30 min in cold acetone, and air dried. Cells were then incubated with PV-1-specific monoclonal antibody C_3 (3) for 30 min at 37°C, washed with PBS, and treated with fluorescein isothiocyanate-labeled anti-mouse gamma globulin for 30 min at 37°C. They were then fixed in formol (4%) for 20 min, mounted in Mowiol, and examined under UV illumination. The percentage of infected cells was determined by scoring at least 1,000 cells for each time point.

Alteration of 160S to 135S particles. HEp-2c cell monolayers (10^7) in 25-cm^2 flasks were chilled for 15 min on ice, washed twice with ice-cold MEM supplemented with 0.5% BSA, and infected with ^{35}S-labeled viruses at an MOI of 30 in 0.8 ml of MEM. Adsorption was allowed to proceed for 90 min at 4°C. The monolayers were then washed twice with ice-cold MEM to remove unbound particles and were further incubated with 5 ml of MEM supplemented with 2% fetal calf serum at 37°C for the times indicated in the legend to Fig. 5. Then, eluted particles were removed by two further washes with ice-cold PBS. Cells were harvested by scraping and suspended in 10 ml of ice-cold PBS without Ca^{2+} or Mg^{2+}. Cells were pelleted by centrifugation and resuspended in 450 μl of 140 mM NaCl–50 mM Tris-HCl, pH 8, and incubated for 10 min in ice. Then, the cells were lysed by adding 50 μl of 140 mM NaCl–10% Nonidet P-40–1% SDS–50 mM Tris-HCl, pH 8, and incubating on ice for 20 min. Cell lysates were clarified by centrifugation for 5 min in an Eppendorf centrifuge. An aliquot of 50 μl of each supernatant was used for measuring cell-associated radioactivity, and the remaining supernatant was layered onto 15 to 30% sucrose gradients prepared in PBS. Gradients were centrifugated in a Kontron TST41 rotor for 2 h at 40,000 rpm at 4°C and fractionated from the bottom by 6-drop fractions in scintillation vials. The amount of ^{35}S label in each fraction was counted. Virus sedimentation markers were prepared by mixing purified radiolabeled virions (160S) with empty capsids (prepared by heating virions for 45 min at 56°C) (80S) in parallel gradients.

Incorporation of [^{3}H]uridine into RNA. HEp-2c cell monolayers (5×10^5) grown in 24-well dishes were washed twice with PBS and were infected in duplicate with viruses at an MOI of 30 in 0.5 ml of MEM supplemented with 0.5% BSA. After a 30-min adsorption period at 37°C, the inoculum was removed and 0.5 ml of MEM containing actinomycin D (5 μg/ml) was added. Twenty microcuries of [^{3}H]uridine (37 Ci/mmol; NEN) per ml was added 90 min postinfection. At the times indicated, the medium was discarded and the cells were lysed in 0.2 ml of 10 mM Tris-HCl (pH 7.5)–1 mM EDTA–0.5% SDS by incubation for 10 min at room temperature. RNAs were precipitated with 10 volumes of 10% trichloroacetic acid. Trichloroacetic acid-insoluble radioactivity was collected on glass-fiber filters (Whatman GF/C) and counted.

Analysis of capsid assembly. HEp-2c cell monolayers (10^7) in 25-cm^2 flasks were rinsed twice with MEM and infected with viruses at an MOI of 20 in 0.8 ml of MEM. After a 30-min adsorption period at 37°C, 1.7 ml of MEM supplemented with fetal calf serum (2%, final concentration) was added. At 3 hpi the cells were washed twice and incubated for 1 h with 15 μCi of [^{35}S]methionine (1,000 Ci/mmol; ICN) per ml in methionine-free medium supplemented with 2% fetal calf serum. Infected cells were lysed and sedimented on sucrose gradients as described for the 160S-to-135S particle assay.

To analyze viral proteins by SDS-polyacrylamide gel electrophoresis (PAGE), infected cells were lysed in 10 mM Tris-HCl (pH 8.0)–1 mM EDTA–140 mM NaCl–0.5% Nonidet P-40 containing protease inhibitors (10 μg of soybean trypsin inhibitor per ml, 2 μg of leupeptin per ml, and 2 μg of aprotinin per ml). Cell lysates corresponding to 2×10^5 cells were clarified for 2 min in an Eppendorf centrifuge and loaded onto a 12.5% polyacrylamide SDS gel.

Thermostability of virus particles. CsCl-purified viruses were diluted in Ca^{2+}- and Mg^{2+}-free PBS to a titer of about 10^8 PFU/ml. Duplicate samples were pipetted into capped glass tubes immersed in a water bath and allowed to incubate either at one of various temperatures for 15 min or at a temperature of 47.5°C for various times. After incubation, the tubes were withdrawn from the water bath and plunged into an ice bath and then stored at −80°C until the end of the experiment. Control samples were pipetted directly into tubes in an ice bath. The infectious titer remaining was determined by $TCID_{50}$ assay at 37°C with HEp-2c cells. Thermolability values represent the difference of the $\log_{10}$ virus titer before and after heating.

RESULTS

Growth characteristics of mouse-adapted mutants KK-$VP1I_{22}$ and KK-$VP2T_{31}$. We determined the plaque morphologies and single-cycle growth curves of mouse-adapted PV-1/Mahoney mutants KK-$VP1I_{22}$ and KK-$VP2T_{31}$ on HEp-2c cells. After 72 h, both mutants formed smaller plaques than did the parental strain PV-1/Mahoney (Fig. 1). The growth kinetics of mutant viruses were assessed as 24-h growth curves. At 1 to 3 h, the titers of mutant KK-$VP2T_{31}$ and particularly of KK-$VP1I_{22}$ were slightly lower than that of PV-1/Mahoney. The

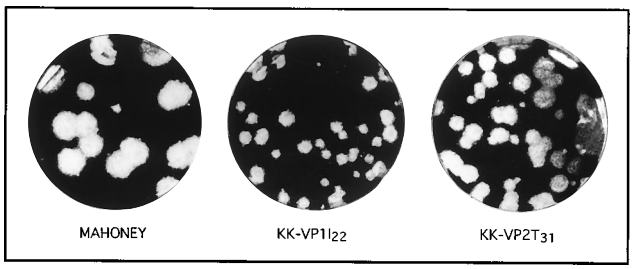

FIG. 1. Plaque phenotypes of wild-type PV-1/Mahoney and mutants KK-VP1I_{22} and KK-VP2T_{31} on HEp-2c cells.

yields of both mutants were three times lower than that of the parental virus (Fig. 2).

Mouse-adapted mutants KK-VP1I_{22} and KK-VP2T_{31} were more rapidly internalized than was PV-1/Mahoney. We measured the binding of radioactive KK-VP1I_{22} and KK-VP2T_{31} virions to HEp-2c cells. The kinetics of adsorption of the mutants and PV-1/Mahoney were similar (data not shown). Thus the substitutions VP1I_{22} and VP2T_{31} did not appear to affect attachment.

The kinetics of internalization of mouse-adapted mutants were then determined with infected HEp-2c cells at an MOI of 50. At various times after infection noninternalized virus was neutralized, and then at 4.5 hpi the cells were examined for the presence of viral antigen by immunofluorescence (Fig. 3). At each time until 60 min postinfection, the percentage of cells infected was higher with KK-VP1I_{22} and KK-VP2T_{31} mutants than with PV-1/Mahoney. The same experiment was performed at an MOI of 100, and the differences between the mutants and the wild-type virus were similar to those observed at an MOI of 50 (data not shown). Thus, the mutations caused improved internalization.

Mouse-adapted mutants KK-VP1I_{22} and KK-VP2T_{31} undergo transitions to 135S particles more rapidly. The pathway

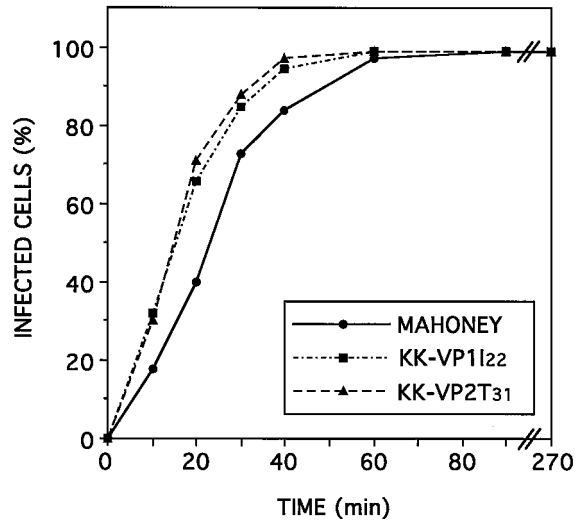

FIG. 3. Kinetics of internalization of PV-1/Mahoney and mutants KK-VP1I_{22} and KK-VP2T_{31}. Monolayers of HEp-2c cells were incubated with 50 PFU of viruses per cell for various periods. At the indicated times, cells were rinsed and anti-PV-1 rabbit serum was added to the culture medium to neutralize noninternalized virus. At 270 min p.i. the cells were examined for the presence of viral antigen by immunofluorescence.

of infection following attachment of PV to PVR involves the formation of 135S particles, which are believed to be a necessary intermediate in the virus-uncoating process (11, 24). We investigated whether differences in the formation of 135S particles account for differences in the kinetics of virus internalization by following the time course of appearance of 135S particles in HEp-2c cells. Infection was first cold synchronized by incubating cells at 4°C with radiolabeled viruses for 90 min. Then, cells were washed to remove all free virus and incubated at 37°C for various periods, after which 160S and 135S particles were assayed as follows. Infected cells were disrupted by de-

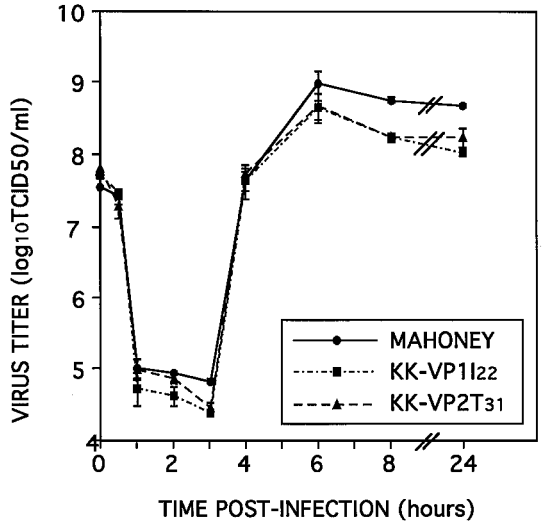

FIG. 2. Single-cycle growth curves of PV-1/Mahoney and mutants KK-VP1I_{22} and KK-VP2T_{31}. HEp-2c cell monolayers were infected (MOI of 50), and after a 30-min adsorption period cells were rinsed and overlaid with growth medium. Cells and supernatants were harvested at the indicated times p.i., and total yield of infective particles was determined by $TCID_{50}$ assay. Each point represents the mean and the standard error of the mean (SEM) (bars) of two separate experiments.

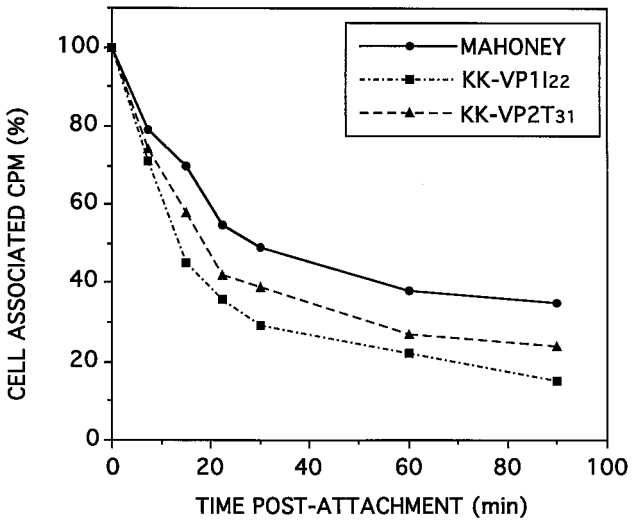

FIG. 4. Kinetics of elution of attached PV-1/Mahoney, KK-VP1I_{22} and KK-VP2T_{31} particles. HEp-2c cells were infected with radiolabeled virus for 90 min at 4°C. Unattached virus was then removed, and cells were incubated at 37°C. Cells were lysed at the indicated times, and cell-associated counts per minute were measured. Time point values are expressed as the percentage of the total counts per minute attached prior to the 37°C incubation.

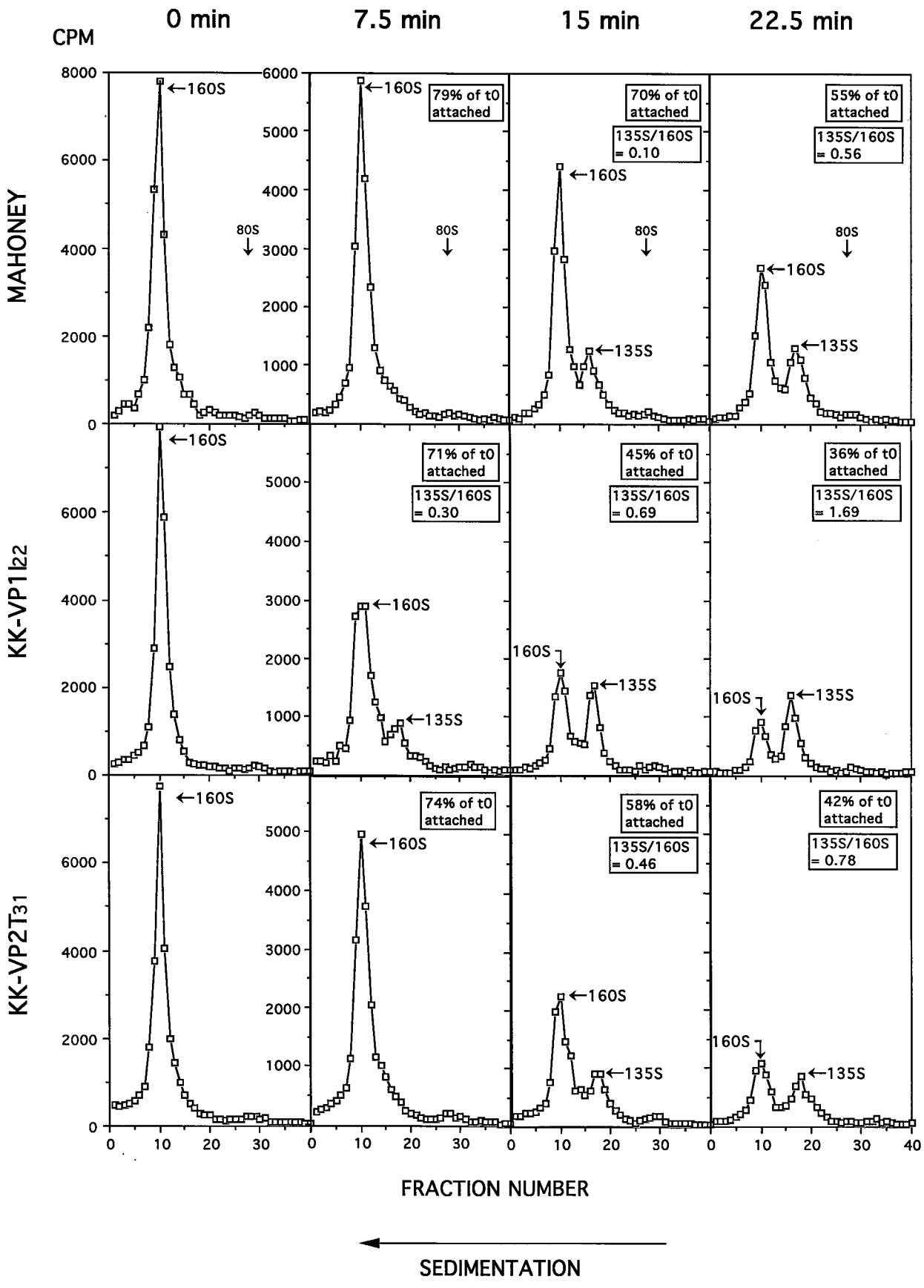
0 min
7.5 min
15 min
22.5 min
CPM
MAHONEY
KK-VP1I22
KK-VP2T31
←160S
←135S
80S
79% of t0 attached
70% of t0 attached
135S/160S = 0.10
55% of t0 attached
135S/160S = 0.56
71% of t0 attached
135S/160S = 0.30
45% of t0 attached
135S/160S = 0.69
36% of t0 attached
135S/160S = 1.69
74% of t0 attached
58% of t0 attached
135S/160S = 0.46
42% of t0 attached
135S/160S = 0.78
FRACTION NUMBER
SEDIMENTATION

FIG. 5. Kinetics of the conversion of 160S virions into 135S particles as analyzed by sucrose gradient centrifugation. Infection of HEp-2c cells with radiolabeled PV-1/Mahoney, KK-VP1I$_{22}$, or KK-VP2T$_{31}$ virus was first synchronized at 4°C. The cells were then incubated at 37°C for the indicated times. After removal of unattached virus, infected cells were lysed and cell-associated particles were sedimented through a 15 to 30% sucrose gradient. The gradients were fractionated from the bottom, and fractions were counted for radioactivity. Purified radiolabeled native (160S) and empty (80S) capsids (prepared by heating virions for 45 min at 56°C) were used as markers in parallel gradients. The percentages of the attached radioactivity at time zero (t0) that remained cell associated after the 37°C incubation are indicated. 135S/160S, the alteration ratio, is the area under the 135S peak divided by the area under the 160S peak.

tergents, the cell-associated radioactivity was measured, and lysates were analyzed by sucrose gradient ultracentrifugation.

After 90 min of incubation at 4°C, the amount of the inoculated virus recovered as cell-associated radioactivity was similar for the three viruses (mean ± standard deviation, 6.58% ± 0.64%). When the infection process was initiated by elevating the temperature from 4 to 37°C, the level of cell-associated radioactivity declined (Fig. 4). This experiment was performed three times for the time points 0, 7.5, 15, and 22.5 min. The percentages of cell-associated counts per minute obtained were similar (with a maximum standard deviation of 2.5%). The decrease of cell-associated radioactivity indicates that a substantial fraction of radioactivity was released into the growth medium. This corresponds to the elution process (12, 15, 19). The elution of both mutants was more substantial than that of PV-1/Mahoney, and the elution of KK-VP1I$_{22}$ was more marked than that of KK-VP2T$_{31}$.

The postadsorption decrease of cell-associated radioactivity was consistent with the decrease of the total amount of radioactivity recovered in the sedimentation profiles (Fig. 5). This experiment was performed three times, and the sedimentation profiles of the cell-associated particles were similar (data not shown). We calculated the distribution of radioactivity between the 160S and 135S fractions for each virus as the alteration ratio (the area under the 135S peak divided by the area under the 160S peak). The alteration ratio is thus a measure of the uncoating transitions. The uncoating transition of KK-VP1I$_{22}$ was earlier (as early as 7.5 min after the shift to 37°C) than that of PV-1/Mahoney. For each time point, the alteration ratio was higher for KK-VP1I$_{22}$ than for PV-1/Mahoney, indicating that KK-VP1I$_{22}$ undergoes the 160S-to-135S transition more efficiently than does PV-1/Mahoney. The alteration ratios for KK-VP2T$_{31}$ were intermediate between those of PV-1/Mahoney and KK-VP1I$_{22}$.

Mouse-adapted mutant KK-VP1I$_{22}$ synthesizes RNA earlier and more efficiently than do PV-1/Mahoney and KK-VP2T$_{31}$. We determined the time course of viral RNA synthesis to investigate whether the more efficient conversion of native virus to 135S particles observed with mutants facilitates RNA release. Virus was attached to cells for 30 min at 37°C. The synthesis of viral RNA over a 10-h period was measured as the cumulative incorporation of [^{3}H]uridine in the presence of actinomycin D (Fig. 6). Viral RNA synthesis by KK-VP1I$_{22}$ was slightly earlier than that by the parental virus. Furthermore, the yield of viral RNA at 8 hpi was larger for KK-VP1I$_{22}$ than for parental virus. Thus, the VP1I$_{22}$ mutation seems to facilitate RNA release. RNA synthesis by KK-VP2T$_{31}$ was similar to that of the parent. Although transitions leading to 135S particles were slightly more efficient with KK-VP2T$_{31}$ than with PV-1/Mahoney, this experiment did not reveal RNA release differences.

Mouse-adapted mutants KK-VP1I$_{22}$ and KK-VP2T$_{31}$ are defective in assembly. Postbinding conformational alteration

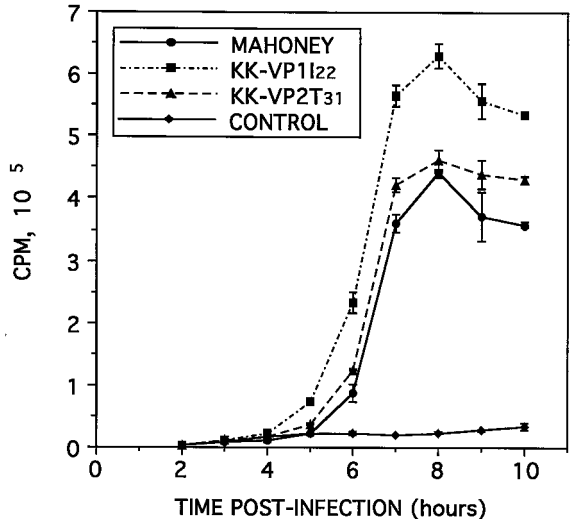

FIG. 6. Time course of total viral RNA synthesis for PV-1/Mahoney, KK-VP1I$_{22}$, or KK-VP2T$_{31}$. Mock-infected cells were used as negative controls. HEp-2c cell monolayers were infected at an MOI of 30, and after a 30-min adsorption period unattached virus was removed and the cells were overlaid with growth medium containing 5 μg of actinomycin D per ml. At 90 min p.i., [^{3}H]uridine (20 μCi/ml) was added to the medium. At the indicated times, cells were lysed, total RNA was precipitated with trichloroacetic acid, and radioactivity was counted. Each point represents the mean value and the SEM (bars) of two separate experiments.

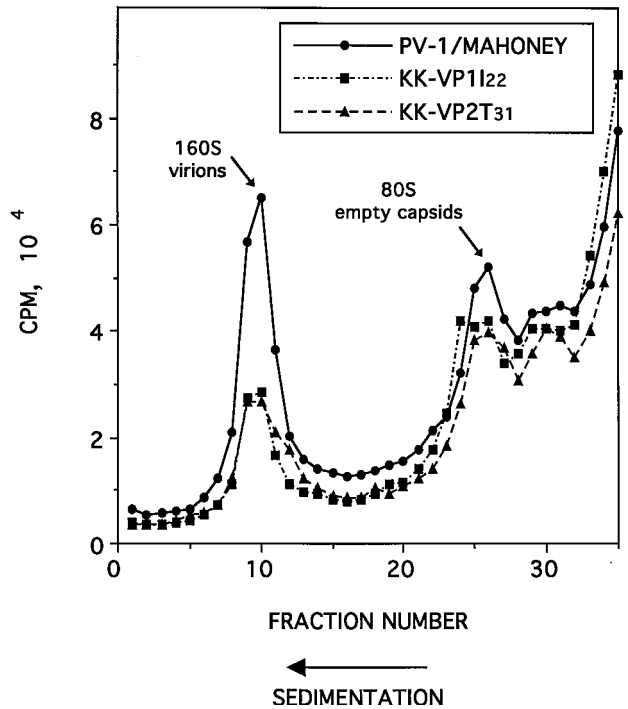

FIG. 7. Analysis of capsid assembly of PV-1/Mahoney and mutants KK-VP1I$_{22}$ and KK-VP2T$_{31}$. After labeling from 3 to 4 hpi, radiolabeled 160S RNA-containing virions and 80S empty capsids accumulated in HEp-2c cells were displayed on sucrose gradients.

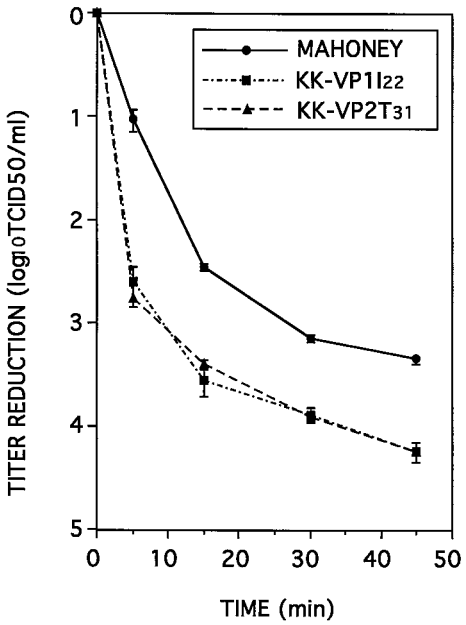

FIG. 8. Temperature-induced inactivation of PV-1/Mahoney and mutants KK-VP1I_{22} and KK-VP2T_{31}. Purified viruses (10^8 PFU/ml of PBS) were heated at 47.5°C for various times, and the titer of infectious virus remaining was measured by $TCID_{50}$ assay. Each point represents the mean value and the SEM (bars) of two separate experiments.

of the mutants KK-VP1I_{22} and KK-VP2T_{31} was more efficient than that of PV-1/Mahoney. However, the yield of both mutants at the end of a single cycle of growth was lower than that of PV-1/Mahoney. To investigate whether this is due to a defect in the formation of infectious viral progeny, we analyzed the distribution patterns of 160S infectious viral particles and 80S RNA-less subviral particles in HEp-2c cells. Infected cell extracts were analyzed by sedimentation on sucrose density gradients following a 1-h labeling period from 3 hpi (Fig. 7). This experiment was performed twice, and the sedimentation profiles were similar (data not shown). Fewer 80S empty particles were observed in mutant cell lysates than in those of PV-1/Mahoney, and the number of mature 160S particles observed for the mutants was very much lower (Fig. 7). Viral proteins from infected cell extracts were examined by SDS-PAGE. The shutoff of cellular proteins was similar for all three viruses. Furthermore, the molecular weights and stoichiometries of viral proteins and the intensities of the corresponding bands were identical for mutants and PV-1/Mahoney (data not shown). Thus, there was no evidence for incorrect synthesis or processing of P1 precursor in the mutants. These results indicate that mutations VP1I_{22} and VP2T_{31} affect the assembly of infectious particles.

Mouse-adapted mutants KK-VP1I_{22} and KK-VP2T_{31} exhibited an altered thermostability. The mutants change conformation efficiently but assemble less efficiently, suggesting instability of the mutant capsids. We examined the temperature-induced inactivation of KK-VP1I_{22} and KK-VP2T_{31} mutants to assess stability. PV-1/Mahoney and mutants were incubated for 15 min at temperatures ranging from 37.5 to 50°C. Differences between thermal inactivation of the mutants and PV-1/Mahoney were largest at 47.5°C (data not shown). We thus chose this temperature to determine the kinetics of thermal inactivation of mutants compared with that of the parental virus (Fig. 8). Viral infectivity of mutants was more sensitive to thermal inactivation than was the infectivity observed with PV-1/Mahoney. Thus, VP1I_{22} and VP2T_{31} substitutions appear to decrease the stability of the virion.

DISCUSSION

Roles of Ile-22 of VP1 and Thr-31 of VP2 during the viral cycle in HEp-2c cells. Mouse adaptation determinants Ile-22 of VP1 and Thr-31 of VP2 were previously mapped to the interior surface of the capsid: residue 22 of VP1 is part of the N-terminal stretch of 31 amino acids which are extruded in the altered 135S particle produced following virion binding to susceptible cells; residue 31 of VP2 abuts a seven-stranded β sheet which forms part of the interface between the pentameric subunits and which is thought to be important to the stability of the infectious virion (9). Furthermore, both residues interact with the polypeptide VP4, which is released during receptor-mediated conformational changes leading to 135S particles. Possibly these and the internal determinants identified in related studies (8, 34) could define a functional area involved in both early steps of the viral cycle and host range restriction in PV (9).

The substitutions Thr-22→Ile and Ser-31→Thr did not affect the binding affinities of mutants for HEp-2c cells. In contrast, kinetic analysis of 160S-to-135S alteration of cell-associated particles provided clear evidence that the substitutions of KK-VP1I_{22} and KK-VP2T_{31} mutants render the receptor-mediated conformational changes leading to the formation of 135S particles more efficient. Furthermore, particle elution from the cell surface during the infection process was greater with mutants than with PV-1/Mahoney. Eluted particles are very similar, if not identical, to intracellular 135S particles (15). Therefore, substitutions rendering the formation of 135S cell-associated particles more efficient may also favor the elution process. Moreover, the elution of KK-VP1I_{22} was greater than that of KK-VP2T_{31}, which was consistent with the more efficient formation of 135S of KK-VP1I_{22}.

Mosser et al. identified mutations in drug-resistant mutants of the Sabin strain of PV-3 mapping in the interior of the capsid, on or near VP4, which conferred a thermolabile phenotype on PV-3 and could predispose the virus to form the 135S particles (35, 36). Mutations VP1I_{22} and VP2T_{31} also map close to VP4. This area thus seems important in the conversion of 160S to 135S particles, presumably being involved in facilitating VP4 release.

The formation of 135S particles is one of the first steps of uncoating, and these particles are considered a necessary intermediate for the entry (penetration and uncoating) of PV (11, 14, 15, 20, 24). Therefore, the improved internalization of mutants KK-VP1I_{22} and KK-VP2T_{31} could be due to the more efficient formation of 135S particles. The kinetics of viral RNA synthesis of at least one of the mutants (KK-VP1I_{22}) appears to reflect more efficient RNA release. It has been shown that mutations in VP4 or in the N terminus of VP1 could specifically affect release of viral RNA without any effect on conformational changes (21, 33). Acquisition of membrane-binding properties by the 135S particle might allow RNA release across the plasma or endosomic membrane via a channel formed by VP4 and the amino termini of VP1 proteins (15, 33). Therefore, the more efficient formation of 135S particles of KK-VP1I_{22} could account for its more efficient viral RNA synthesis. Viral RNA synthesis by mutant KK-VP2T_{31} was similar to that of the Mahoney strain. This may be due to the less efficient 160S-to-135S conversion of KK-VP2T_{31} particles than that of KK-VP1I_{22} particles. Alternatively, residue VP1I_{22} may be directly involved in the formation of 135S particles and RNA

release, and $VP2T_{31}$ may be involved only in formation of 135S particles.

The substitutions $VP1I_{22}$ and $VP2T_{31}$ also caused defects in mutant assembly. The pleiotropic character of these substitutions suggests linked mechanisms involving capsid stability, consistent with the results of the thermolability assay. The increased propensity to undergo the conformational changes seems to be associated with a more marked defect in assembly, explaining the lower yields of both mutants during single-growth cycle and the small-plaque phenotype. The small-plaque phenotype could also be due to greater elution of the mutants from the cell surface. Given the results of single-cycle growth and plaque morphology, the differences observed between mutants KK-$VP1I_{22}$ and KK-$VP2T_{31}$ during early steps (formation of 135S and RNA synthesis) of the viral cycle did not appear to have repercussions on the virus yield.

Roles of Ile-22 of VP1 and Thr-31 of VP2 in the mouse-adapted phenotype. Residues Ile-22 of VP1 and Thr-31 of VP2 confer on PV-1/Mahoney the ability to infect the mouse central nervous system. Our findings show that these residues play similar roles during the viral cycle on HEp-2c in the conversion to 135S particles. Foot-and-mouth disease virus, another picornavirus, is able to bind in an antibody-dependent manner to the Fc receptor expressed by Chinese hamster ovary cells and to infect these cells productively (28). In contrast, PV-1 binds to these cells via the Fc receptor but there is no subsequent viral replication (28). Moreover, it has been shown that PV can specifically attach to proteins on the surface of cultured mouse cells but cannot initiate infection in the absence of human PVR (1, 28). It seems, therefore, that efficient PV infection of cells requires not only binding but also altered 135S particle formation as an intermediate during the uncoating process. This results from interaction between the virion and its receptor molecule on the cell surface. Although we cannot investigate the viral replication of mutants on permissive mouse cells, we can assume that the entry of PV into mouse nerve cells requires a process similar to that leading to 135S particles in HEp-2c cells. These determinants might, therefore, confer the mouse-adapted phenotype by allowing more efficient conformational change. Moss and Racaniello (34) identified an internal determinant of mouse adaptation of PV-1 (residue 54 of VP1), and Mosser et al. (36) have shown that the corresponding residue of PV-3 increases capsid thermolability, suggesting that it could predispose the virus to formation of the 135S particles, like $VP1I_{22}$ and $VP2T_{31}$.

Our analysis of the early steps of the viral multiplication cycle of the mouse-adapted PV-1/Mahoney mutants suggests a model in which both PV-1/Mahoney and mouse-virulent mutants are able to attach to murine receptors but only the mutants are able to overcome the block during early steps of the mouse nerve cell infection. They could do so by efficiently undergoing conformational changes required for subsequent steps. RNA release was more efficient than that for the wild type for only one mutant. Thus, the only critical stage involved in mouse adaptation seems to be the alteration of 160S to 135S particles, leading to a more efficient internalization. These destabilizing mutations which render one of the first steps of uncoating more efficient decrease the assembly and stability of virions. Therefore, these mouse adaptation determinants seem to control the delicate balance between the need for structural stability and the requirement for the ability to undergo the conformational changes mediated by the murine nerve cell receptor.

ACKNOWLEDGMENTS

We are grateful to F. Colbère-Garapin for critical reading of the manuscript.

This work was supported by grants from the Institut National de la Santé et de la Recherche Médicale (CRE 911301 and 910107) and from the Association Française contre les Myopathies (contract 3720).

REFERENCES

1. **Barnert, R. H., H. Zeichhardt, and K. O. Habermehl.** 1992. Identification of 50-kDa and 23-/25-kDa HeLa cell membrane glycoproteins involved in poliovirus infection—occurrence of poliovirus specific binding sites on susceptible and nonsusceptible cells. Virology **186:**533–542.
2. **Blondel, B., R. Crainic, O. Fichot, G. Dufraisse, A. Candrea, M. Girard, and F. Horaud.** 1986. Mutations conferring resistance to neutralization with monoclonal antibodies in type 1 poliovirus can be located outside or inside the antibody-binding site. J. Virol. **57:**81–90.
3. **Blondel, B., O. Akacem, R. Crainic, P. Couillin, and F. Horodniceanu.** 1983. Detection by monoclonal antibodies of an antigenic determinant critical for poliovirus neutralization present on VP1 and on heat inactivated virions. Virology **126:**707–710.
4. **Colonno, R. J., J. H. Condra, S. Mizutani, P. L. Callahan, M. E. Davies, and M. A. Murcko.** 1988. Evidence for the direct involvement of the rhinovirus canyon in receptor binding. Proc. Natl. Acad. Sci. USA **85:**5449–5453.
5. **Colston, E., and V. R. Racaniello.** 1994. Soluble receptor-resistant poliovirus mutants identify surface and internal capsid residues that control interaction with the cell receptor. EMBO J. **13:**5855–5862.
6. **Colston, E. M., and V. R. Racaniello.** 1995. Poliovirus variants selected on mutant receptor-expressing cells identify capsid residues that expand receptor recognition. J. Virol. **69:**4823–4829.
7. **Couderc, T., T. Barzu, F. Horaud, and R. Crainic.** 1990. Poliovirus permissivity and specific receptor expression on human endothelial cells. Virology **174:**95–102.
8. **Couderc, T., N. Guédo, V. Calvez, I. Pelletier, J. Hogle, F. Colbère-Garapin, and B. Blondel.** 1994. Substitutions in the capsids of poliovirus mutants selected in human neuroblastoma cells confer on the Mahoney type 1 strain a phenotype neurovirulent in mice. J. Virol. **68:**8386–8391.
9. **Couderc, T., J. Hogle, H. Le Blay, F. Horaud, and B. Blondel.** 1993. Molecular characterization of mouse-virulent poliovirus type 1 Mahoney mutants: involvement of residues of polypeptides VP1 and VP2 located on the inner surface of the capsid protein shell. J. Virol. **67:**3808–3817.
10. **Dietzschold, B., T. J. Wiktor, J. Q. Trojanowski, R. I. Macfarlan, W. H. Wunner, M. J. Torres-Anjel, and H. Koprowski.** 1985. Differences in cell-to-cell spread of pathogenic and apathogenic rabies virus in vivo and in vitro. J. Virol. **56:**12–18.
11. **Everaert, L., R. Vrijsen, and A. Boeyé.** 1989. Eclipse products of poliovirus after cold-synchronized infection of HeLa cells. Virology **171:**76–82.
12. **Fenwick, M. L., and P. D. Cooper.** 1962. Early interactions between poliovirus and ERK cells. Some observations on the nature and significance of the rejected particles. Virology **18:**212–223.
13. **Filman, D. J., R. Syed, M. Chow, A. J. Macadam, P. D. Minor, and J. M. Hogle.** 1989. Structural factors that control conformational transitions and serotype specificity in type 3 poliovirus. EMBO J. **8:**1567–1579.
14. **Flore, O., C. E. Fricks, D. J. Filman, and J. M. Hogle.** 1990. Conformational changes in poliovirus assembly and cell entry, p. 429–438. *In* J. M. Hogle (ed.), Seminars in virology. W. B. Saunders Co., London.
15. **Fricks, C. E., and J. M. Hogle.** 1990. Cell-induced conformational change in poliovirus: externalization of the amino terminus of VP1 is responsible for liposome binding. J. Virol. **64:**1934–1945.
16. **Gomez Yafal, A., G. Kaplan, V. R. Racaniello, and J. M. Hogle.** 1993. Characterization of poliovirus conformational alteration mediated by soluble receptors. Virology **197:**501–505.
17. **Hogle, J. M., M. Chow, and D. J. Filman.** 1985. Three dimensional structure of poliovirus at 2.9 Å resolution. Science **229:**1358–1365.
18. **Holland, J. J.** 1961. Receptor affinities as major determinants of enterovirus tissue tropisms in humans. Virology **15:**312–326.
19. **Joklik, W. K., and J. E. Darnell.** 1961. The adsorption and early fate of purified poliovirus in HeLa cells. Virology **13:**439–447.
20. **Kaplan, G., M. S. Freistadt, and V. R. Racaniello.** 1990. Neutralization of poliovirus by cell receptors expressed in insect cells. J. Virol. **64:**4697–4702.
21. **Kirkegaard, K.** 1990. Mutations in VP1 of poliovirus specifically affect both encapsidation and release of viral RNA. J. Virol. **64:**195–206.
22. **Koike, S., H. Horie, I. Ise, A. Okitsu, M. Yoshida, N. Iizuka, K. Takeuchi, T. Takegami, and A. Nomoto.** 1990. The poliovirus receptor protein is produced both as membrane-bound and secreted forms. EMBO J. **9:**3217–3224.
23. **Koike, S., C. Taya, T. Kurata, S. Abe, I. Ise, H. Yonekawa, and A. Nomoto.** 1991. Transgenic mice susceptible to poliovirus. Proc. Natl. Acad. Sci. USA **88:**951–955.
24. **Lonberg-Holm, K. L., L. B. Gosser, and J. J. Kauer.** 1975. Early alteration of poliovirus in infected cells and its specific inhibition. J. Gen. Virol. **27:**329–342.
25. **Lonberg-Holm, K. L., L. B. Gosser, and E. J. Shimshick.** 1976. Interaction of

liposomes with subviral particles of poliovirus type 2 and rhinovirus type 2. J. Virol. **19:**746–749.
26. **Lu, H.-H., C.-F. Yang, A. D. Murdin, M. H. Klein, J. J. Harber, O. M. Kew, and E. Wimmer.** 1994. Mouse neurovirulence determinants of poliovirus type 1 strain LS-a map to the coding regions of capsid protein VP1 and proteinase $2A^{pro}$. J. Virol. **68:**7507–7515.
27. **Martin, A., C. Wychowski, T. Couderc, R. Crainic, J. Hogle, and M. Girard.** 1988. Engineering a poliovirus type 2 antigenic site on a type 1 capsid results in a chimeric virus which is neurovirulent for mice. EMBO J. **7:**2839–2847.
28. **Mason, P. W., B. Baxt, F. Brown, J. Harber, A. Murdin, and E. Wimmer.** 1993. Antibody-complexed foot-and-mouth disease virus, but not poliovirus, can infect normally insusceptible cells via the Fc receptor. Virology **192:**568–577.
29. **Melnick, J. L., H. A. Wenner, and C. A. Philips.** 1979. Enteroviruses, p. 471–534. *In* E. H. Lennette and N. J. Schmidt (ed.), Diagnostic procedure for viral, rickettsial and chlamydial infections. American Public Health Association, Washington, D.C.
30. **Mendelsohn, C., B. Johnson, K. A. Lionetti, P. Nobis, E. Wimmer, and V. R. Racaniello.** 1986. Transformation of a human poliovirus receptor gene into mouse cells. Proc. Natl. Acad. Sci. USA **83:**7845–7849.
31. **Mendelsohn, C. L., E. Wimmer, and V. R. Racaniello.** 1989. Cellular receptor for poliovirus: molecular cloning, nucleotide sequence and expression of a new member of the immunoglobulin superfamily. Cell **56:**855–865.
32. **Morrison, M. E., and V. R. Racaniello.** 1992. Molecular cloning and expression of a murine homolog of the human poliovirus receptor gene. J. Virol. **66:**2807–2813.
33. **Moscufo, N. A., A. Gomez Yafal, A. Rogove, J. M. Hogle, and M. Chow.** 1993. A mutation in VP4 defines a new step in the late stages of cell entry by poliovirus. J. Virol. **67:**5075–5078.
34. **Moss, E. G., and V. R. Racaniello.** 1991. Host range determinants located on the interior of the poliovirus capsid. EMBO J. **10:**1067–1074.
35. **Mosser, A. G., and R. R. Rueckert.** 1993. WIN 51711-dependent mutants of poliovirus type 3: evidence that virions decay after release from cells unless drug is present. J. Virol. **67:**1246–1254.
36. **Mosser, A. G., J. Y. Sgro, and R. R. Rueckert.** 1994. Distribution of drug resistance mutations in type 3 poliovirus identifies three regions involved in uncoating functions. J. Virol. **68:**8193–8201.
37. **Murray, M. G., J. Bradley, X. F. Yang, E. Wimmer, E. G. Moss, and V. R. Racaniello.** 1988. Poliovirus host range is determined by a short amino acid sequence in neutralization antigenic site 1. Science **241:**213–215.
38. **Olson, N. H., P. R. Kolatkar, M. A. Oliveira, R. H. Cheng, J. M. Greve, A. McClelland, T. S. Baker, and M. G. Rossmann.** 1993. Structure of a human rhinovirus complexed with its receptor molecule. Proc. Natl. Acad. Sci. USA **90:**507–511.
39. **Ren, R. B., F. Costantini, E. J. Gorgacz, J. J. Lee, and V. R. Racaniello.** 1990. Transgenic mice expressing a human poliovirus receptor: a new model for poliomyelitis. Cell **63:**353–362.
40. **Rueckert, R. R.** 1976. On the structure and morphogenesis of picornaviruses, p. 131–213. *In* H. Fraenkel-Conrat and R. Wagner (ed.), Comprehensive virology. Plenum Press, N.Y.
41. **Shepley, M. P., and V. R. Racaniello.** 1994. A monoclonal antibody that blocks poliovirus attachment recognizes the lymphocyte homing receptor CD44. J. Virol. **68:**1301–1308.